Rodrigues et al. BMC Zoology (2016) 1:3
DOI 10.1186/s40850-016-0005-7

BMC Zoology

RESEARCH ARTICLE Open Access

The cellular basis of bioadhesion of the freshwater polyp *Hydra*

Marcelo Rodrigues[1*], Philippe Leclère[2], Patrick Flammang[3], Michael W. Hess[4], Willi Salvenmoser[1], Bert Hobmayer[1] and Peter Ladurner[1*]

Abstract

Background: The freshwater cnidarian *Hydra* temporarily binds itself to numerous natural substrates encountered underwater, such as stones, leafs, etc. This adhesion is mediated by secreted material from specialized ectodermal modified cells at the aboral end of the animal. The means by which *Hydra* polyps attach to surface remain unresolved, despite the fact that Hydra is a classic model in developmental and stem cell biology.

Results: Here, we present novel observations on the attachment mechanism of *Hydra* using high pressure transmission electron microscopy, scanning electron microscopy, atomic force microscopy, super-resolution microscopy, and enzyme histochemistry. We analyzed the morphology of ectodermal basal disc cells, studied the secreted material, and its adhesive nature. By electron microscopy we identified four morphologically distinct secretory granules occurring in a single cell type. All the secretory granules contained glycans with different distribution patterns among the granule types. Footprints of the polyps were visualized under dry conditions by atomic force microscopy and found to consist of a meshwork with nanopores occurring in the interstices. Two antibodies AE03 and 3G11, previously used in cell differentiation studies, labelled both, basal disc cells and footprints. Our data suggest that the adhesive components of *Hydra* are produced, stored and delivered by a single cell type. Video microscopy analysis corroborates a role of muscle contractions for the detachment process.

Conclusion: We clearly demonstrated that bioadhesion of *Hydra* relies on the secreted material. Our data suggest that glycans and/or glycoproteins represent an important fraction of the secreted material. Detachment seems to be initiated by mechanical forces by muscular contractions. Taken together, our study represents the characterization of an unique temporary adhesive system not known in aquatic organisms from other metazoan phyla.

Keywords: Hydra, Basal disc, Biological adhesion, Adhesion

Background

Aquatic organisms, freshwater and marine, have evolved a myriad of effective solutions for underwater adhesion. Cases range from microscopic organisms, such as bacteria, through much larger and complex marine algae, invertebrates, and vertebrates. Examples include the permanent attachments of sessile mussels [1] and barnacles [2, 3], the temporary attachment of starfish and flatworms during locomotion [4, 5], the construction of protective shelters by sandcastle worms [6], and the defence against predators by the Cuverian tubules of sea cucumbers [7]. All these bioadhesives were adapted by natural selection for specific roles in the organism's life style. Likewise, the way they attach are also remarkably complex and involve a large range of interactions and components with different functions [8, 9]. Generally, these multicomponent adhesives are composed of protein, carbohydrates, and inorganic components. The amount of each component is highly variable in different organisms. For instance, in sea stars 21 % are proteins, 8 % carbohydrates, and 40 % inorganic material [10]. On the contrary, in barnacles 90 % of the adhesive is made out of proteins with the remainder being 1 % carbohydrates, 1 % lipids, and 4 % inorganic material [11]. Mussels have one of the best studied bioadhesive systems [12, 13]. These marine molluscs routinely stick to all kinds of surfaces underwater using their so-called byssus. This structure consists of a protein complex

* Correspondence: marcelo.rodrigues@uibk.ac.at; peter.ladurner@uibk.ac.at
[1]Institute of Zoology and Center for Molecular Biosciences Innsbruck, University of Innsbruck, Innsbruck, Austria
Full list of author information is available at the end of the article

secreted as a fluid that spreads spontaneously and exhibits strong reversible interfacial bonding and tunable cross-linking. Similarly, the sabelariid polychaete sandcastle worm *Phragmatopoma californica* [6, 14] secretes micro-droplets of adhesive to build a tube-like burrow from sand grains and other particles. Alternatively, the marine flatworm *Macrostomum lignano*, possesses a duo-gland adhesive system in the tail plate [5] that allows it to adhere and release from the substrate multiple times within seconds. The different characteristics of all these adhesives are often derived from the physico-chemical properties of the adhesive proteins, and in particular, from their post-translational modifications (PTM), such as hydroxylation, phosphorylation, and glycosylation [15, 16]. Some organisms contain glycans associated with the adhesive proteins, but it is unknown whether they are covalently attached to the proteins [10, 17].

The freshwater cnidarian *Hydra* (Fig. 1a, b) is a solitary polyp inhabiting any unpolluted body of shallow freshwater all year round. During its whole lifecycle it lives temporarily attached underwater, being able to attach and detach repetitively, but only detaching when looking for better living conditions [18]. Reproduction is sexual and/or by asexual budding which dominates when food is plentiful. The fertilized egg develops into an embryo that grows to an adult polyp, or as late blastula enters a resting stage surrounded by a chitinous covering. The animal has a single axis and consists of only two layers of epithelial cells: the endoderm and the ectoderm [19]. At the oral end is the hypostome (mouth opening), which is surrounded by a ring of tentacles, and at the aboral end is an adhesive disc called "basal disc" [20]. It is well known that basal disc cells are derived from ectodermal cells of the lower gastric column [21, 22], therefore consisting of modified ectodermal cells that secrete an adhesive material by which *Hydra* can attach strongly to a number of surfaces underwater, i.e., stones, wood sticks, leaves, and other submerged parts of plants.

Hydra is a classical model organism in axial pattern, regeneration, and stem cell biology [22–26]. In contrast to the existing detailed information about differentiation and regeneration of the ectodermal basal disc cells, only few studies have addressed *Hydra's* astonishing attachment ability. The ultrastructure of ectodermal basal disc cells was studied by Chaet [27] and Philpott et al. [28] who provided a first description of *Hydra*'s secretory granules. They placed these granules in three categories, two of them representing the same type of granule in different stages of matureness, while the third granule is of a different type. Further, Davis [29] proposed that basal disc cells produce, by themselves or jointly with other cells, at least six types of granules, and a seventh one that originates from the neighbouring digestive cells. The only constituent identified inside the basal disc cells is the presence of hyaluronic acid as seen after an Alcian Blue [28, 29] and PAS staining [28]. At the ultrastructural level, granules between 0.5 and 1.5 μm in diameter are known to be peroxidase positive [30]. The mode of action and the components of the secreted adhesives are not understood. Enlarged cytoplasmic protrusions which were named as filopodia were observed during *Hydra* attachment by Pan et al. [31].

In this study, our goal was to characterize the cellular components responsible for *Hydra*'s underwater adhesion. Light-and electron microscopic techniques were utilised for a comprehensive description of basal disc morphology of free and attached polyps. Additionally, morphology and adhesiveness of the secreted material (footprint) was analysed using atomic force microscopy. To investigate the components involved in adhesion, we first used energy electron loss spectroscopy to identify nitrogen and phosphorus atom distribution. Second, the periodic acid-Schiff reaction was carried out to verify the presence of glycans, and diamino benzidine was used to attest peroxidase activity. The localisation of two antigens labelled by two antibodies was confirmed to be present in the footprints. Finally, we showed that lipids most probably do not play a role in *Hydra* adhesion. We suggest that detachment is driven by muscular activity. After investigating all these components, we paved the way for *Hydra* as a model organism for bioadhesion research using molecular approaches [32]. It provides the basis for our current efforts to uncover the biochemical basis of the glue of *Hydra*.

Results

Basal disc cell morphology and secretion of adhesive granules

Using interference contrast microscopy of squeezed live animals the basal disc cells can be seen at the aboral end of the animal (Fig. 1c and d). A longitudinal section through a Carnoy-fixed unattached polyp showed an overview of the basal disc cells, which constitute the adhesive system (Fig. 1e and f). The external morphology of the basal disc consisted of a cylindrical peduncle covered by a flat disc (Fig. 2a). Between the basal disc cells there were uniformly distributed pores (Fig. 2b). Secreted material was visible on the basal disc (Fig. 2c). In a *Hydra* polyp attached to the substrate (Fig. 3a and b), the basal disc cells appeared directly in contact with the surface. When it detached, it left behind a footprint made up of the secreted material on the surface (Fig. 3c). The basal disc cells left behind an imprint outlining their apical cell-to-cell contact sites. The flat zones between the rims outlining the basal disc cells also contain a thin film of adhesive material (see below). In summary, the basal disc is a specialized secretory tissue allowing *Hydra* to attach to the surface.

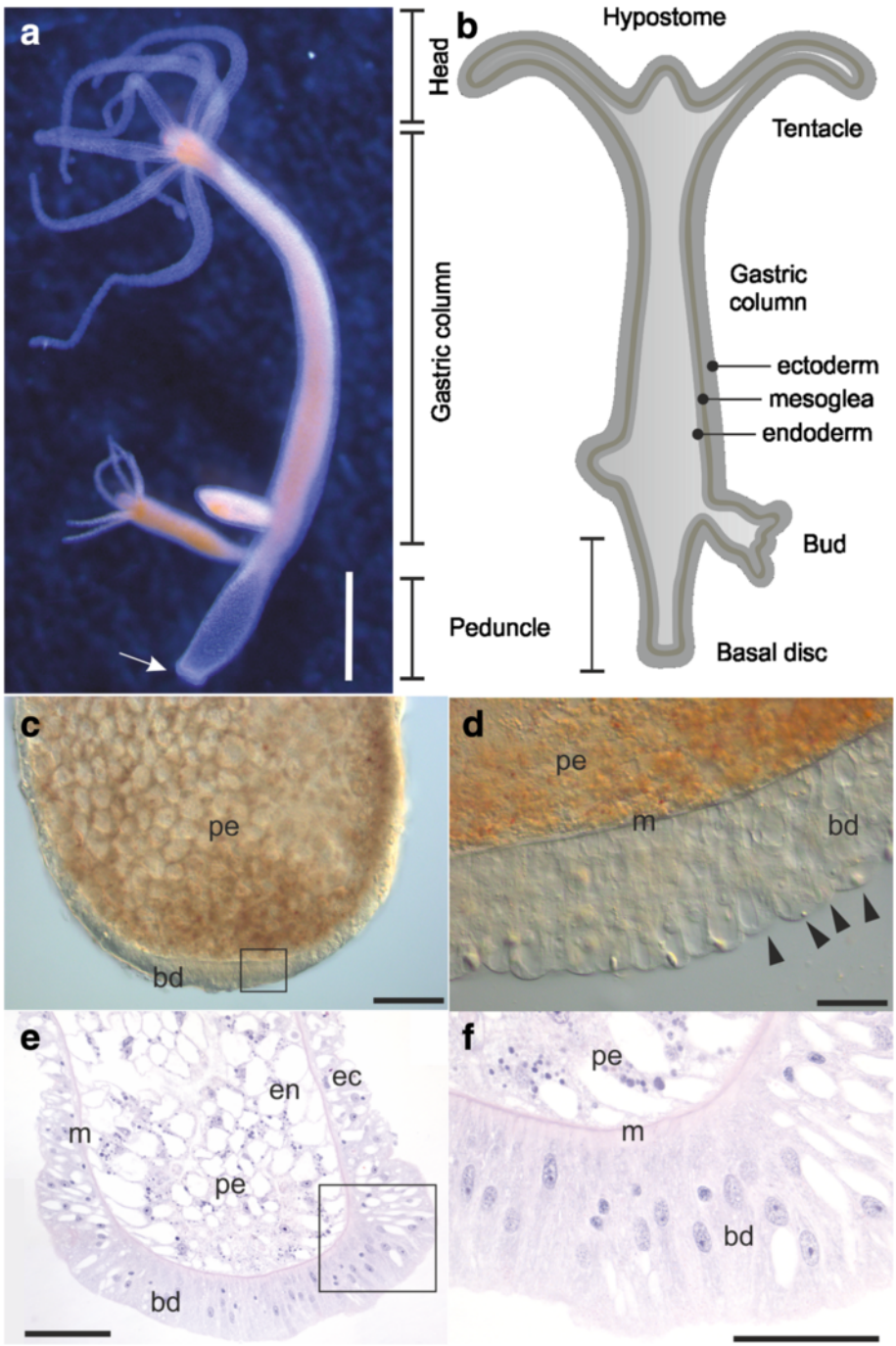

Fig. 1 Light microscopy images of live and fixed *Hydra magnipapillata* strain 105. **a** An adult polyp. The arrow indicates the basal disc. **b** Scheme of an adult polyp indicating details of the animal morphology. **c** Squeezed preparation of the foot region. The square indicates the area magnified in figure **d**. **d** The arrowheads point at individual basal disc cells. **e** Longitudinal section stained with hematoxylin eosin showing a general morphology of the basal disc. Inset shows the zone magnified in figure **f**. **f** Organization of basal disc cells with stained nuclei. Scale *bars* 1 mm (**a**), 100 μm (**c**), 50 μm (**d**-**f**). *Abbreviations*: ec, ectoderm; m, mesoglea; en, endoderm; pe, peduncle; bd, basal disc

The detachment process was recorded with video microscopy (Additional file 1). In the beginning, the full basal disc was attached. The polyp started the detachment from the outer rim towards the center of the basal disc. When the detachment got closer to the center, *Hydra* suddenly detached the last cells. A footprint was left behind which was transparent underwater (Additional file 1). Phalloidin staining revealed the actin filament distribution

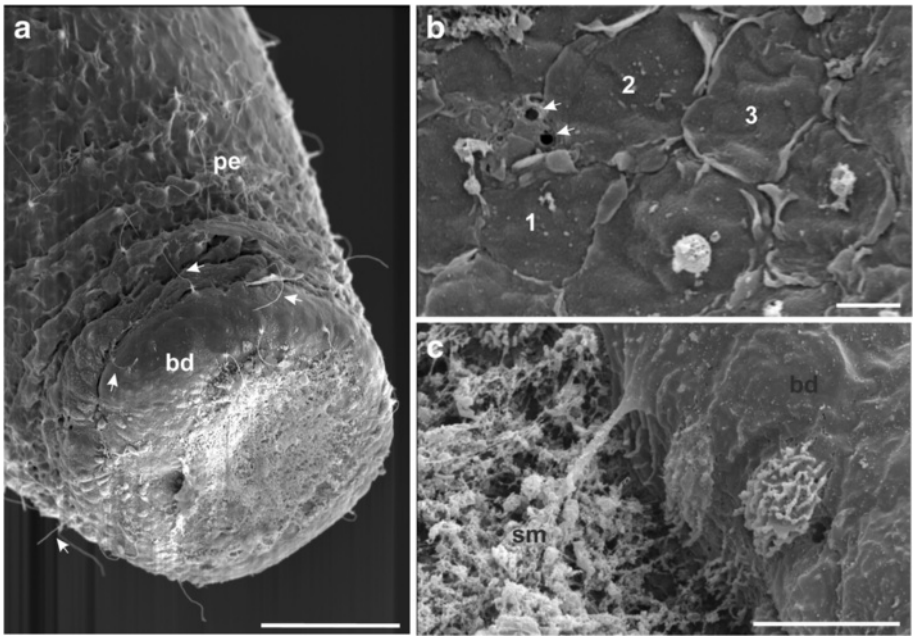

Fig. 2 Scanning Electron Microscopy. **a** Outer aspect of the basal disc. Arrows point at discharged nematocysts. **b** Basal disc surface. The numbers 1, 2, 3, mark three different basal disc cells. Arrows point at pores between the cells. **c** basal disc and substrate covered with secretory material. *Scale bars* 100 μm (**a**), 2 μm (**b**), 10 μm (**c**). *Abbreviations*: pe, peduncle; bd, basal disc; sm, secretory material

in the basal disc (Additional file 2). Within the ectodermal layer the myonemes were radially distributed (Additional file 2: Figure S2 a and b). From the radial myonemes a branch of myonemes goes perpendicularly towards the apical side of ectodermal basal disc cells (Additional file 2: Figure S2 c). This distribution of myonemes was corroborated by transmission electron microscopy experiments (Additional file 3: Figure S3 a). Within the endodermal layer they were circular (Additional file 2 Figure S2 a and b). Based on these observations, we propose that muscle contractions of the two cell layers (ectoderm and endoderm) of the basal disc were involved in the detachment of the animals.

In side view at the ultrastructural level, the basal disc cells had an irregular rectangular-like shape with a planar diameter ranging from 10 to 17 μm at the apical end of the cell and an apical-basal diameter about 51 to 60 μm (Fig. 4a). Several water containing vacuoles were seen as major constituents of the cells (Fig. 4 and Additional file 3: Figure S3 b). Their most apical region, which actually gets in contact with the surface when attached (Fig. 4c and d), beared an array of protruded cytoplasmic extensions with a diameter of about 0.4–1 μm. Filopodia-like cytoplasmic extensions were observed to be in contact with the surface after basal disc attachment (Fig. 4d, and Additional file 3: Figure S3 b). Basal disc cells presented many morphological characteristics of gland cells. The cells cytoplasm was rich in endoplasmic reticulum (ER), golgi fields, and mitochondria around the stored secretory granules. Based on morphology and size, four types of granules located close to the secretory cell membrane could be discriminated (Fig. 4b and Additional file 3: Figure S3 b). First, *Hydra* secretory granules I (HSGI) are likely precursor (maturing granules) of the granules HSGII (Additional file 3: Figure S3 c). These maturing granules were closely associated with ER, suggesting that these organelles are involved in the synthesis and/or maturation of the secretory granule contents. HSGI measured between 1.90 and 2.10 μm in diameter, and their content were electron lucent. Second, *Hydra* secretory granules II (HSGII) represented electron dense granules with a diameter ranging from 0.40 to 1.10 μm. *Hydra* secretory granules III (HSGIII) measured between 0.45 and 0.49 μm in diameter, and appeared less electron dense than the *Hydra* secretory granules IV (HSGIV). HSGIV were by far the smallest granules with a diameter of 0.18 to 0.21 μm (Fig. 4b). In thick sections of 350 nm, secretory granules can be seen overlapping each other, corroborating that these are true vesicles (Additional file 3: Figure S3 b). Besides the granules membrane, there was no compartmentation of adhesive components inside the cell at any stage of the secretory process, and there was no intracellular drainage system. Once the cell surface established contact with the substratum (Fig. 4c), the basal disc cells secreted the adhesive material by exocytosis. The secreted material was deposited as a thin film filling any space between the cells and the substratum (Fig. 4d and see also AFM Fig. 5). This film gives rise to the footprint after detachment.

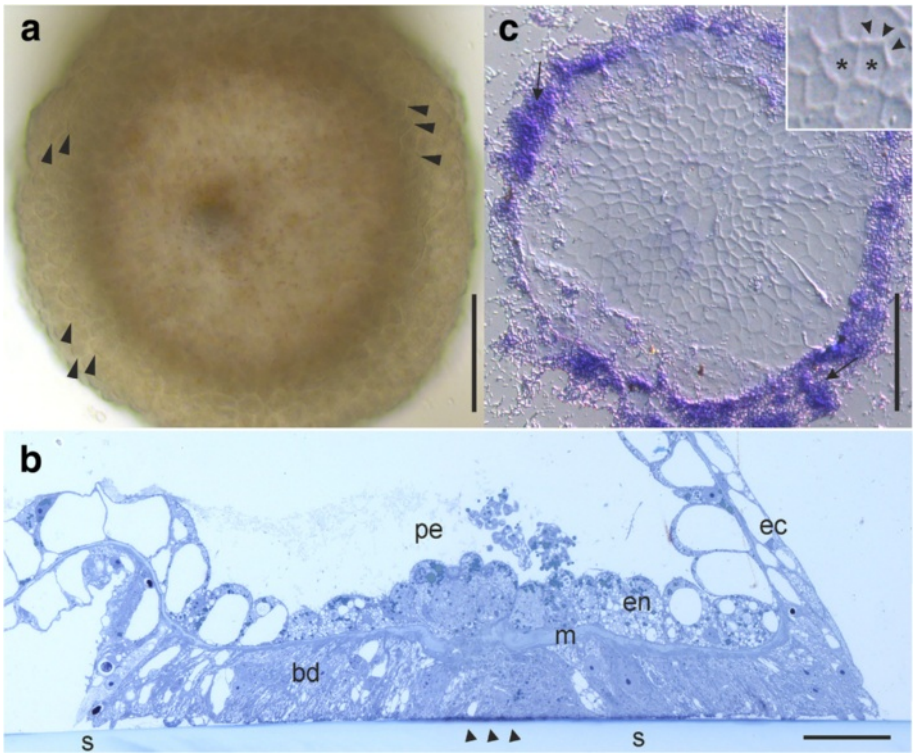

Fig. 3 Light microscopy images of live (**a**) and fixed-attached *Hydra* polyp (**b**), and secreted footprint (**c**). **a** Overview of the basal disc of a live attached polyp taken through inverted microscopy. Individual basal disc cells (arrowheads) are in focus along the outer margin. **b** Longitudinal semi-thin section stained with the basic dye methylene blue and Azur II. The polyp was chemically-fixed when still attached to a substratum. *Arrowheads* indicate the interface between substratum and polyp where the adhesive is secreted. **c** Footprint deposited by the basal disc of a *Hydra* polyp stained with crystal violet. Imprints derived from individual cells are visible in the centre of the footprint while at the periphery fungi can be observed [*arrows*]. Inset is a magnification of a central area of the footprint where the flat area [*asterisks*] and the rims [*arrowheads*] can be seen in a better detail. The fungi are contamination and/or symbionts of *Hydra* culture. *Scale bars* 100 μm (**a**, **c**), 50 μm (**b**). *Abbreviations*: s, substratum; bd, basal disc; ec, ectoderm; m, mesoglea; en, endoderm; pe, peduncle

Overall, our results confirm that the basal disc cells produce secretory granules and that their contents play the core role in *Hydra* adhesion.

The air dried footprints were easily located using phase contrast and could be precisely positioned beneath the AFM cantilever. Care was taken to select a scan site near to the rim of the footprints and to avoid regions that were too thick to image. When visualized through AFM, the footprints of *Hydra* were found to be a meshwork with nanopores occurring in the interstices of the deposited material (Fig. 5a). The secreted material seems homogeneous, traces of individual secretory granules cannot be detected. Several pores of about 0.5–1 μm where present at the surface of the footprint whose diameter correlated to the one of the protruded cytoplasmic extensions. The adhesion profile (Fig. 5b) showed that adhesive forces were higher in the deeper (thinner) areas of the footprint, reaching up to 66.4 nN. In summary, the AFM results corroborate the adhesive nature of the secreted material.

Chemistry of granules

To determine whether granules contained vicinal diol-containing glycans, Periodic Acid Schiff (PAS) cytochemistry was carried out in both light-and electron microscopy. The PAS method positively stained basal disc cells showing a gradient towards the apical end of the cells. The strongest reaction was observed most apically where the granule secretion takes place (Fig. 6a and b). Figure 6c showed that HSGII were fully positive to PAS, with a strongest reaction near their surrounding membrane, while negative control did not show any staining (Fig. 6d). HSGIII and IV, positively reacted throughout the whole vesicle. Alcian blue staining was negative for ectodermal basal disc cells in *H. magnipapillata* at pH-value 2.5. As positive control reaction for AB we successfully stained nematocysts in tentacles sections (Additional file 4), validating that the method used was functional. Our results showed that secretory granules from *H. magnipapillata* contained neutral glycans instead of the acidic compounds found previously in other species.

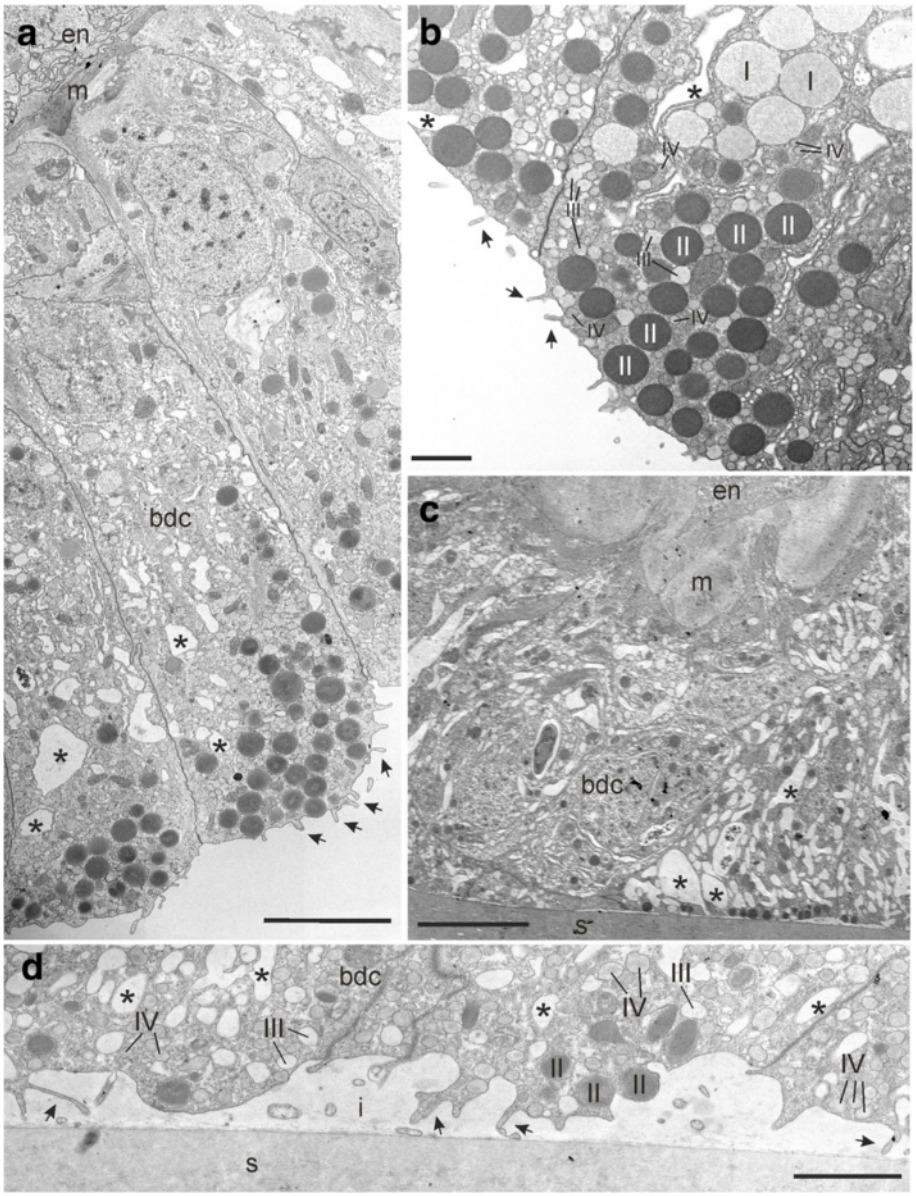

Fig. 4 Transmission electron microscopy images of chemically and cryo-fixed *Hydra* polyps. **a** Longitudinal section through a chemically-fixed basal disc showing individual basal disc cells. Electron dense granules tend to accumulate at the aboral end of the cell, which is the area attaching to the substratum. At the aboral end, several cytoplasmic extensions are present [*arrows*]. **b** Cryo-fixed basal disc reveals the fine structure of secretory granules. **c** Chemically-fixed *Hydra* polyp right after attachment to the substratum. **d** Interface between an attached basal disc and the substratum. Note protruded cytoplasmic extensions are in contact with the substratum. *Scale bars* 10 μm (**a**, **c**), 2 μm (**b**), 5 μm (**d**). *Abbreviations*: en, endoderm; m, mesoglea; bdc, basal disc cell; I, *Hydra* secretory granule I; II, *Hydra* secretory granule II; III, *Hydra* secretory granule III; IV, *Hydra* secretory granule IV; s, substratum; *arrows*, indicate cytoplasmic extensions; *asterisks*, indicate vacuoles of water

Diamino benzidine treated polyps allowed to visualize peroxidase activity in the basal disc of *Hydra* (Fig. 6e and f). The reaction was stronger close to where exocytosis takes place. The peroxidase reaction was associated with HSGI (Fig. 6g and h), but not for all the granules. Peroxidase activity was also detected at the level of cytoplasmic components surrounding HSGII.

Based on information from other model organisms, in which lipids played an important role in adhesion [33, 34], the occurrence of lipids was investigated in the present study using Nile Red on *Hydra* whole mounts. When exposing stained specimens to both blue (450–500 nm) and green (550 nm) exciting light, dispersed droplets of lipids measuring between 1 and 1.8 μm were visible in basal disc cells (Additional file 5), but apparently not associated to

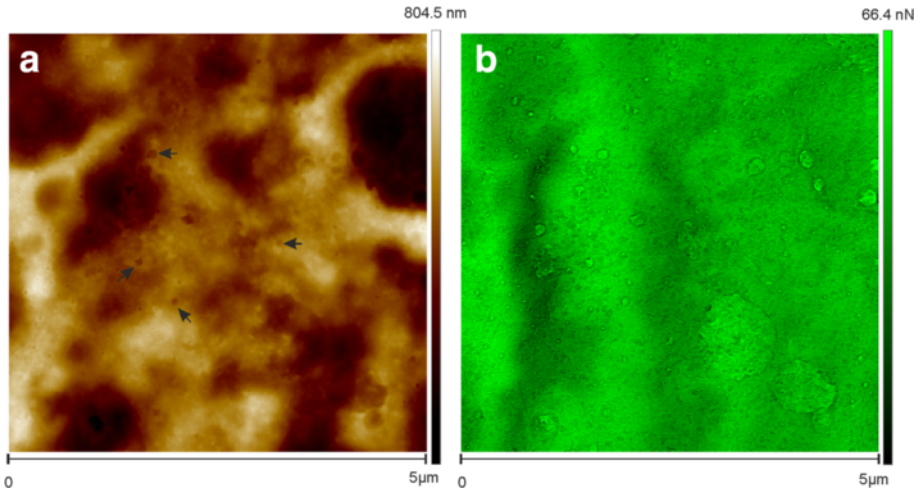

Fig. 5 Atomic force microscopy images collected in air on dried footprints from *Hydra*. **a** Height profile revealing the meshwork structure. *Arrows* point at pores presumably corresponding to cytoplasmic before polyp detachment. **b** Adhesion profile

secretory granules. Lipid droplets were also not observed in the footprints (data not shown). Therefore, these results support a view that lipids do not play a critical role in the adhesion process of *Hydra*.

Electron energy loss spectroscopy (EELS) and electron spectroscopic imaging (ESI) experiments allowed to determine the distribution of nitrogen and phosphorus on high-pressure freezing ultrathin resin sections from cryofixed specimens. Among the secretory granules, high contents of N atoms were found in HSGI and II (Additional file 6), demonstrating their protein nature. P atoms were observed in HSGI and II (Additional file 6) although at a lower density when compared to N atoms. In summary, EELS and ESI showed the presence of proteins and potentially post-translationally modified by phosphorylation, in some granules of basal disc.

Two monoclonal antibodies had been previously applied to study nematocyte development [35] and basal disc cell differentiation [36, 37]. Notably, both antibodies also stained secreted material, however, this aspect was not further pursued in the earlier studies. Therefore, we applied immunohistochemistry with antibodies AE03 [35, 36], and 3G11 [37] to label basal disc cells in whole mount preparations or macerated single cells, and of footprints. Both antibodies were confirmed to label the basal disc of polyps as well as the secreted material (Fig. 7a-h). AE03 also recognized nematoblasts and mature nematocytes [35], but this immunoreactivity did not impede the present study which focused at basal disc cells and their secretion. In super-resolution microscopy images, AE03 showed a clear specificity to an inner ring of granular structures (Fig. 7c) whereas 3G11 also recognized granular structures as well as cytoplasmic constituents throughout the whole cell (Fig. 7g). However, we cannot infer which granule type was labelled with the antibodies. Although in macerated cells the staining patterns of the two antibodies were different, the pattern appeared very similar in the footprint (Fig. 7d and h). The stained pattern of secreted material with a densely stained rim outlining the cell margins and a weaker stained flat centre, corroborates our earlier observation of a crystal violet stained footprint (Fig. 3c). Therefore, our results confirm that the granule material is in fact secreted by basal disc cells.

Discussion

Hydra is considered to represent the most basal animals with a defined body plan and organized epithelia. A common feature within the cnidarian group is their ability of producing bioadhesives either for attaching permanently or temporarily to surfaces through specialized ectodermal cells, and their ability for food capture through specialized nematocysts. Here we investigated the ability of temporary adhesion in *Hydra* through ectodermal basal disc cells (Fig. 8) which represents one of the most ancient metazoan ways of cell-to-surface adhesion.

In organisms well-known for their capacity to adhere temporarily, such as free living flatworms [5] and sea stars [10] the adhesive mechanism relies on a duo-gland system where two or more secretory cell types collaborate in a way that allows attachment and detachment by using adhesive and de-adhesive components. The number of cell types are variable, free living flatworms enclose one adhesive and one de-adhesive cell, while sea stars have two adhesive and one de-adhesive cell type. Some parasitic flatworms possess two different glands producing dissimilar adhesive components, while cells producing de-adhesive constituents are absent [38]. In contrast, substrate detachment in *Hydra* is mediated by differentiated epithelia muscle cells of the ectoderm of

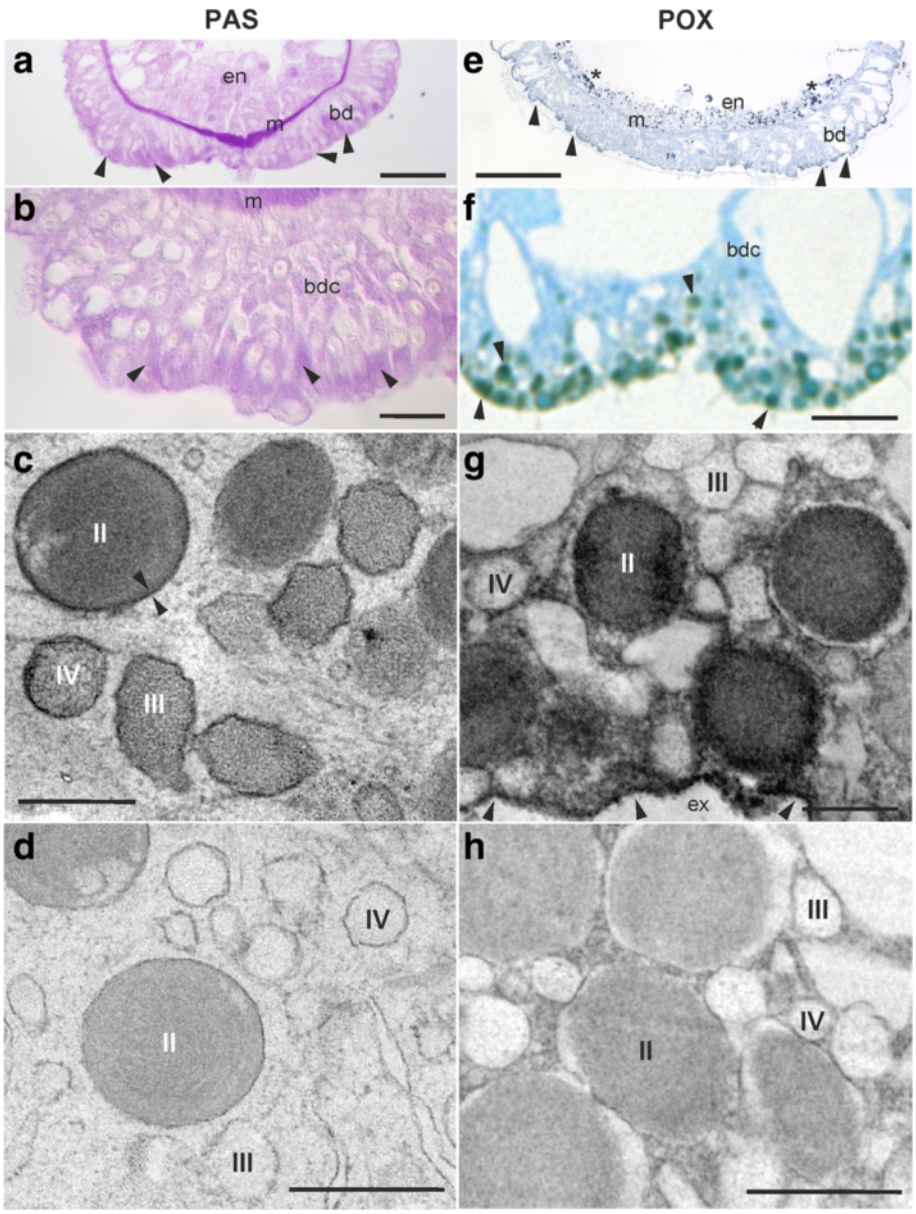

Fig. 6 Cytochemistry of *Hydra* basal disc. **a** Overview of semi-thin Epon section stained for glycans with PAS method. The reaction is stronger in the mesoglea and at the aboral tip [*arrows*] of the cell. **b** Magnification of **a**. *Arrows* indicate strong PAS reactions. Note the reaction gets stronger towards the aboral end of basal disc cells. **c** TEM- Periodic acid-thiocarbohydrazide-silver proteinate reaction (the EM-correlate PAS staining) was performed on cryo-fixed basal disc revealing the glycan distribution in the *Hydra* secretory granules. HSGII react positively in and close proximities of the granule membrane, while HSGIII and IV reacts quite uniformly. **d** Basal disc section not exposed to Periodic acid but regular thiocarbohydrazide-silver proteinate staining. Note secretory granules do not react to glycan staining. **e** Longitudinal semi-thin section through the basal disc stained with diamino benzidine and oxidized with Osmiun tetroxide. Endogenous peroxidase activity is strong at the aboral end of the basal disc [*arrows*] and endodermal lipid granules are dark from osmium fixation [*asterisks*]. **f** Longitudinal section of basal disc cells reacted for peroxidase after diamino bencidine staining counterstained with methylene blue and Azur II. *Arrows* point at some reacted secretory granules located at the most-aboral end of the cells. **g** TEM-peroxidase staining in chemically fixed basal disc is positive for some *Hydra* secretory granules II and their neighbouring cytoplasm. Arrows point at the most aboral end cell membrane, region with highly peroxidase activity. **h** Section from a negative control not exposed to diamino benzidine. *Scale bars* 100 μm (**a**), 50 μm (**b**, **e**), 20 μm (**f**), 1 μm (**c**, **d**, **g**, **h**). *Abbreviations*: PAS, periodic acid Schiff; POX, peroxidase; en, endoderm; m, mesoderm; bd, basal disc; bdc, basal disc cell; I, *Hydra* secretory granule I; II, *Hydra* secretory granule II; III, *Hydra* secretory granule III, IV, *Hydra* secretory granule IV; ex, exterior of the cell

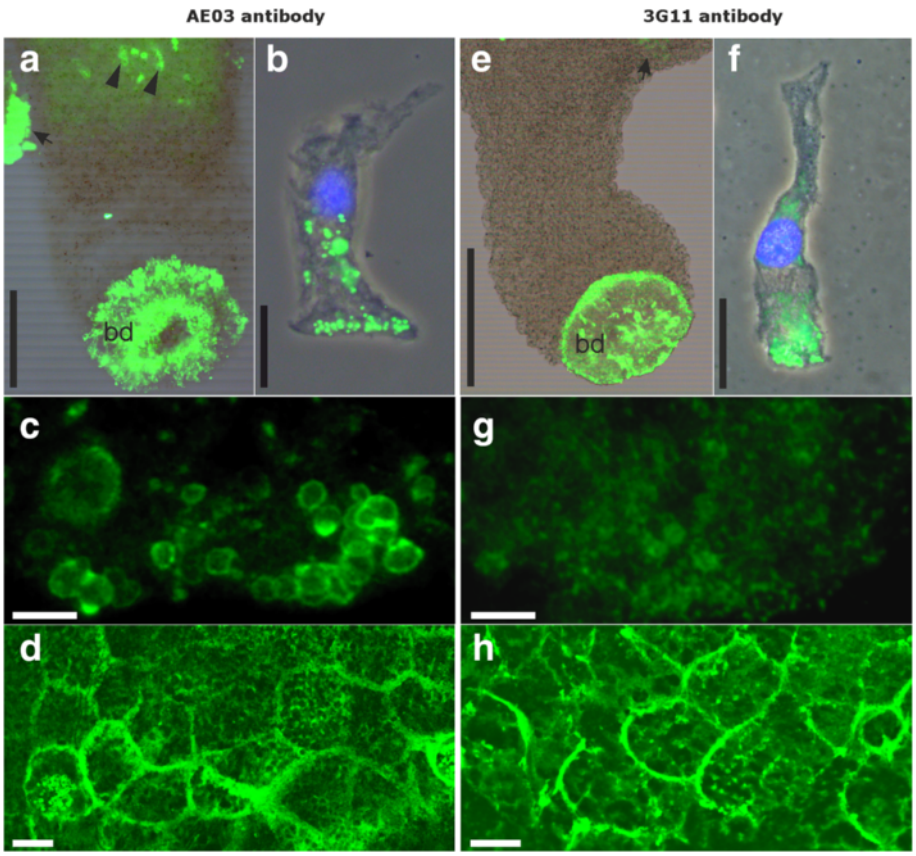

Fig. 7 Immunofluorescence staining of whole mount (merged bright field and fluorescence), macerated cell (merged phase contrast and fluorescence), and footprints with anti-AE03 and 3G11 antibodies. **a** Whole mount, **b** Macerated basal disc cell, **c** apical side of macerated cell imaged with super-resolution microscopy, and **d** footprint stained with AE03 antibody. **e** Whole mount, **f** macerated basal disc cell, **g** apical side of macerated cell imaged with super-resolution microscopy and **h** footprint stained with 3G11 antibody. Both AE03 and 3G11 have affinity to basal disc cells. Their corresponding antigens are eventually secreted and become a component of the adhesive anchoring *Hydra* polyps underwater. *Scale bars* 200 μm (**a**), 10 μm (**b**, **f**), 1 μm (**c**, **g**), 15 μm (**d**, **h**), 400 μm (**e**). Abbreviations: bd, basal disc; *arrows*, indicate bud; *arrowheads*, indicate nematocysts

basal disc. EM observations on secretory granules morphology in these cells [28, 29] with additional information on the molecules present. We have identified four morphologically distinct secretory granules (HSGs) as a major component of the basal disc cells that could be involved in adhesion although it remains unclear to which degree each granule type contributes to the adhesion process. We classified the HSGII as a mature granule derived from the HSGI, because these two granules share biochemical features, they are the only ones of protein nature, and contain phosphor. We also observed possible transition stages from HSGI to HSGII. Another feature is that HSGI is never seen close to the most-apical side of the cell. However, we have no direct proof for granule maturation. Therefore, this process must be further addressed in order to understand granule development.

The component that is actually labeled by the antibodies was not precisely identified. However, super-resolution microscopy experiments (Fig. 7d and h) showed that both antibodies stained granular structures that are eventually secreted and become a constituent of the secreted material. The footprint of *Hydra* is a meshwork of quite homogenous strands. The starfish and sea cucumber footprint have a similar meshwork morphology [7, 39], but contain globular nanostructures which are absent in *Hydra*. In the case of *Hydra*, all HSG have spherical morphology before release and are not recognizable in the footprint. The contents of the granules seem to have merged or fused into larger aggregates forming the strands. In the footprints of sea cucumber [7], adhesive forces of 17nN were measured under dry conditions, and for the rootlets of the English ivy [40] 298 nN. Our measurements of *Hydra* footprints showed an adhesion force as high as 66 nN. Measurements in natural *Hydra* living conditions (i.e., under freshwater) would be necessary for a better understanding of its footprint adhesion forces. Yet, despite repeated attempts, the topographical visualization of the footprints under

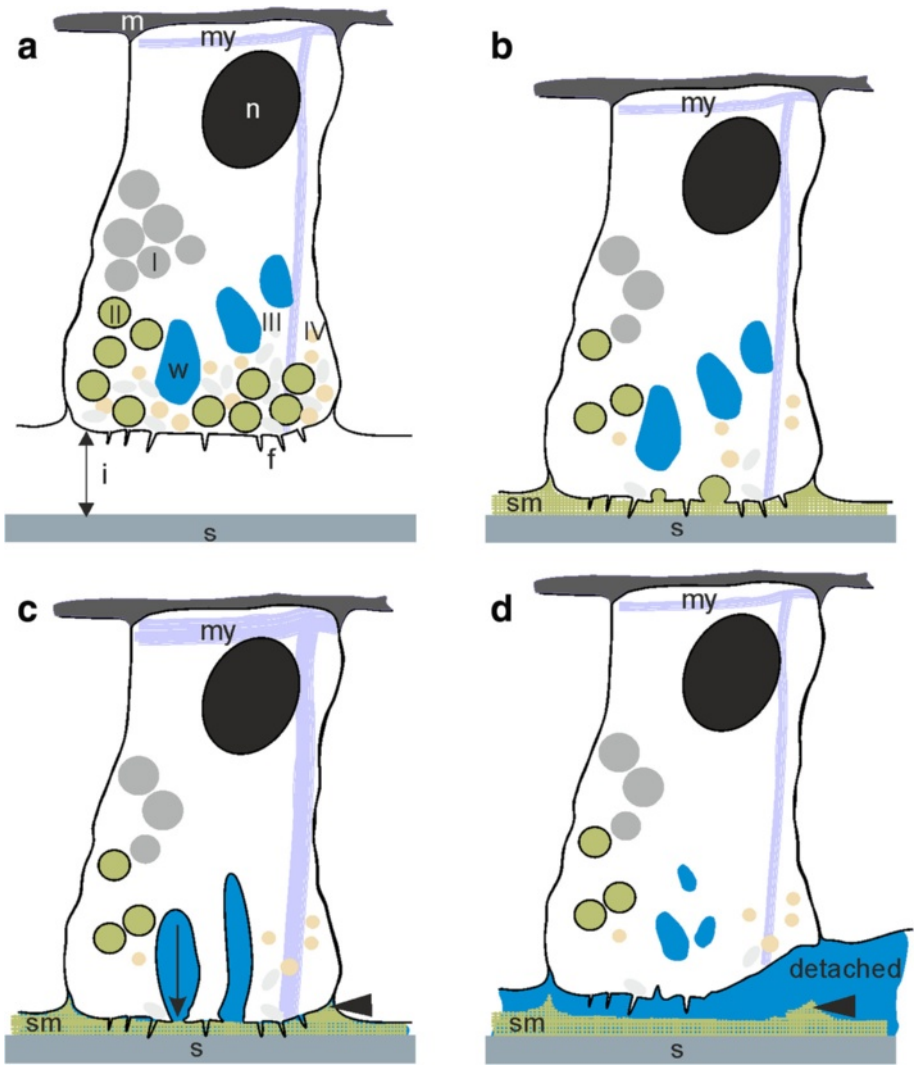

Fig. 8 Schematic representation of attachment (**a**-**c**) and detachment (**d**) of *Hydra*. Arrowheads indicate rims of footprints. Abbreviations: m, mesoglea; n, nucleus; my, myoneme; w, vacuoles of water; I-IV, *Hydra* secretory granule types; i, interface; s, substratum; f, cytoplasmic extensions; sm, secreted material; fo, footprint

native conditions in culture medium was not possible, due to the transparent nature of the footprints. New technical developments would be needed to provide an appropriate contrast for identifying the footprint underwater.

Glycans are considered important components for temporary adhesives, e.g., in cephalopods, gastropods, and echinoderms [10, 17, 41–43]. Permanent glues seems to be generally composed mainly of protein. Glycans have not been considered as an important moiety, though reported from mussels, stalked and acorn barnacles, sandcastle worms, and caddisfly larva [2, 11, 44, 45]. Although previous reports showed alcian blue staining of basal disc cells of other *Hydra* species [28, 29], our alcian blue experiments performed at pH-value 2.5, staining was negative for *H. magnipapillata*. In *Hydra*, EM cytochemistry showed that glycans occur in all the HSG, with differential distributions (the present study). The presence of phosphor (P) in HSGI and II raises the question about possible protein phosphorylation of the *Hydra* adhesive. Phosphorus in the form of phosphate group may indeed be involved in phosphorylation, a PTM which confer additional functionalities to proteins, including adhesive proteins [16]. Phosphoproteins have been identified in a number of aquatic adhesives, e.g., in adults and larvae of barnacles [3, 34], in the caddisfly larvae [46], in mussels [47], in sandcastle worms [48], in sea cucumbers [16], and in kelp spores [49]. Although, covalently attached phosphate groups are usually present at substoichiometric levels (less than 5 % of the protein is modified) in intracellular proteins [50, 51], their proportion is usually much higher in extracellular structural proteins such as adhesive proteins. For instance, in Pc3 an adhesive

protein from the sandcastle worm, up to 90 mol% (residues per 100 residues) of the serine residues are modified by phosphorylation [48]. The P concentration observed within HSGII (Additional file 6) is lower than that of N (Additional file 6). Both, glycosylation and phosphorylation, could be important in the adhesion process of *Hydra*.

Peroxidase activity in the basal disc of *Hydra* [52, 53] has been used as an important biochemical marker for tracking the reappearance of basal disc cells during polyp regeneration [53]. The *Hydra* genome [54] encodes five isoforms of putative peroxidases. Their functional significance for the animal is still under debate [55, 56], but most likely they play several roles. The obtained results are similar to the ones described earlier for other *Hydra* species [30]. Although peroxidase-like enzymes are highly concentrated in basal disc cells, it is not the adhesive *per se*, and its role in *Hydra's* adhesion remains to be elucidated. The peroxidase-like enzyme could catalyse the crosslinking of other components to post-draw the secreted adhesive as it occurs in the freshwater caddisfly silk [57]. Furthermore, it is well known that peroxidase-like enzymes possess antimicrobial features [58], and can function to either foster beneficial relationships or control pathogenesis. During the attachment process, the basal disc secretes a protein-rich adhesive material which might serves as a nutrient source for bacteria and the peroxidase may have a protective role, reducing bacterial biodegradation over the time protein needs for curing. The combination of both functions, i.e., curing and antimicrobial, may occur in *Hydra* adhesion, though the functional significance of this is yet to be examined.

In various organisms, detachment from temporary adhesion is controlled by additional secretory products, enzymes, or by creating forces. However, the detachment processes are largely not well understood. The observations on *Hydra* presented here support the hypothesis that its detachment is mechanically induced (Additional files 1 and 2). If chemical detachment were the case, the basal disc would detach at once, and individual basal disc cells would not be seen detaching individually. When detachment is necessary, myonemes within both ectoderm (radial myoneme) and endoderm (circular myoneme) composing the basal disc contract, leading to an expansion of both radial and circular myonemes. This retracts the attached cells from the surface that in combination with the longitudinal myonemes contracting the vacuoles of water which expels water into the footprint meshwork would pull the polyp off the cured adhesive.

Conclusion

This study showed that cnidarian *Hydra* polyps secrete elaborate adhesive composites underwater (freshwater) to temporarily anchor themselves to substrate surfaces. The adhesive system used by *Hydra* exhibits unique features among metazoans. Glue based adhesion is the main component of the system: basal disc cells release their adhesive vesicles whose contents would have the ability to spread over the surface, displace water, and create a proper environment for curing the secreted glue. Projecting structures were observed, but the way they functions is enigmatic. The adhesive components of *Hydra* are produced, stored and delivered by a single cell type, the ectodermal basal disc cells. Our results revealed that the secretory granules contained glycans and phosphorus, which are important components in other bioadhesive systems. A Peroxidase-like enzyme was associated with secretory granules and could play a role in *Hydra* adhesion. This work was intended to offer a first overview of the *Hydra* adhesive system. The characteristics presented here provide a basis for an ongoing project aimed at unravelling the molecular components of *Hydra'* glue.

Methods

Animals

Hydra magnipapillata strain 105 was used for all the experiments carried out in this study in compliance with animal welfare laws and policies (Austrian Law for animal experiments, TVG 2012, §1). Permanent mass cultures were bred and kept at 18 °C in growth chambers, and day/night light cycle at the Institute of Zoology, University of Innsbruck. *Hydra* cultures were fed five times per week with freshly hatched *Artemia* nauplii as previously described [59]. Under these conditions, animals remained asexual and reproduced by budding. We selected animals that had at least one bud. Animals were starved for 24 h before experiments. Before fixation, animals were relaxed in 2 % urethane in culture medium for 2 min.

Light microscopy

For bright field or differential interference contrast visualization, processed samples were examined with a Leica DM5000. Images were taken with a Leica DFC495 digital camera and a Leica LAS software.

Footprint: To collect *Hydra*'s footprints, polyps were placed onto glass slides and allowed attach for 30 min. After this period, polyps were gently detached with the help of a glass pipet. Glass slides bearing footprints were rinsed three times with *Hydra* culture medium before staining. Fresh footprints were stained using a 0.05 % solution (in culture medium) of Crystal Violet, and rinsed in culture medium.

Squeezing preparations: Living polyps were anesthetized in a 2:1 mixture of 2 % Urethane and culture medium, transferred in a drop onto a slide and slightly squeezed under a coverslip. The specimens were observed with interference contrast under the same microscopy as mentioned above.

Histology: Adult *Hydra* polyps were fixed in Carnoy's fixative (ethanol, chloroform, glacial acetic acid, 6 + 3 + 1 respectively), Bouin's fluid (saturated picric acid, 36 % formaldehyde, and glacial acid, 15 + 3 + 1 respectively), 4 % paraformaldehyde (PFA) in 0.1 M Phosphate Buffer (PBS)) and/or in Flemmings fixative (1 % chromium (VI) oxide, 2 % osmium tetroxide and glacial acetic acid, 15 + 4 + 1 respectively), dehydrated and embedded into paraplast or in Technovit 7100 resin. Paraplast sections (7 μm) and resin sections (3 μm) were produced with a Reichert Autocut 2030 (Reichert, Austria) and stained with hematoxylin and eosin (HE), periodic acid Schiff (PAS), or alcian blue (AB) pH 2.5.

Enzymehistochemistry: For peroxidase activity, *Hydra* polyps were fixed with 4 % PFA in 0.1 M PBS, stained with diamino benzidine (DAB + CHROMOGEN, Dako) post fixed either with 2.5 % glutaraldehyde or 1 % osmium tetroxide, dehydrated and embedded in PolyBed 812 resin. Semi thin sections (350 nm to 500 nm) were cut with a Leica ultra-microtome UCT (Leica, Austria) and stained according to Richardson et al. [60].

Lipid staining: PFA fixed polyps were stained with the fluorescence Nile Red method as whole mounts for lipid detection following method used by Gohad et al. [34]. Negative controls were performed by exposing specimens to ETOH washes. Whole mounts were visualized under a Leica SP5 II confocal laser scanning microscope.

Antibody staining

Two antibodies labelling basal disc cells were used: AE03 [35, 36], and 3G11 [37] were kindly provided by the corresponding authors. The antibody staining method was slightly modified from the original protocols. Experiments were performed on whole mount, macerated cells and footprints. Samples were mounted in Vectashield (Vector), and visualized with a Leica DM5000, or a Leica SP5 II confocal scanning microscope. For super resolution microscopy, macerated cells samples were mounted in Mowiol and examined with a Leica TCS SP8 gSTED microscope system. Obtained super-resolution images were deconvoluted using the Huygens software from Scientific Volume Imaging implemented in the TCS SP8.

Whole mount preparation: For AE03 labelling, whole polyps were fixed in Zamboni's fixative (2 % PFA, 0.2 % picric acid in 0.1 M PBS pH 7.2). For 3G11 labelling, whole polyps were fixed in 4 % PFA. Both fixations were done at 4 °C overnight. The following steps were applied to both antibodies: After three washes with PBS, the polyps were permeabilized with 0.5 % Triton in PBS for 30 min, and incubated with 0.5 % Triton, 1 % bovine serum albumin (BSA, w/v) in PBS with primary antibody (dilutions = AE03 1:5, and 3G11 1:1000) overnight at 4 °C. After this period, polyps were washed three times in PBS, and incubated for 2 h with fluorescein isothiocyanate-conjugated (FITC) antimouse lgG (Dako) secondary antibody (1:200). Polyps were washed again three times in PBS and mounted.

Macerated cells: Basal discs (from approx. 150 polyps) were excised and incubated in 200 μl maceration medium (acetic acid, glycerol, and distilled water, 1:1:7) for 2 h at 30 °C. Basal discs were then mechanically disrupted by shearing them through the opening (roughly 1 mm diameter) of a pipette. The same amount of fixative, either Zamboni or PFA, were added to the medium containing cells and gently mixed. 50 μl of the sample were spread onto gelatine-coated slides and allowed dry for 20 min at RT. Steps for antibody staining were as for whole mount. Differences were a Triton concentration of 0.1 %, and an incubation time for the secondary antibody of 4 h. Slides were additionally counterstained with the DNA-specific fluorochrome, Hoechst 33342 (Life Technologies; 1 μg/ml). Samples examined with super-resolution microscopy were incubated with antimouse abberior STAR 488 (Abberior) secondary antibody diluted 1:100.

Footprint: Secreted material was collected on glass slides as described for light microscopy purposes. Immunofluorescence staining with AE03 and 3G11 was carried out as described above.

We tried to elucidate the subcellular binding of AE03 and 3G11, but several different immunogold approaches failed: i) post-embedded immunogold on both, cryo and chemically fixed material [61], ii) post-embedded immunogold on thawed cryosections according Tokuyasu [62], and iii) pre-embedded with horseradish labelled streptavidin conjugated antibodies.

Phalloidin staining

Configuration of actin filaments in the basal disc were detected by phalloidin staining. Experiments were performed using amputated basal discs. Animals were let to attach to a glass slide for approximately 1 h and were then amputated. Basal discs were fixed with 4 % PFA for 1 h at room temperature, then washed three times for 10 min in PBS-0.5 % Triton, and then incubated in Alexa 488 phalloidin (Invitrogen) in a concentration of 1:400 for 1 h at RT in the dark. Afterwards, they were washed three times for 10 min with PBS. Samples were mounted in Vectashield (Vector), and visualized with a Leica SP5 II confocal scanning microscope.

Scanning electron microscopy

Hydra polyps were fixed in 4 % PFA for 24 h. They were dehydrated in graded ETOH, dried by the critical point method (with CO_2 as transition fluid), mounted on aluminium stubs, coated with gold in a sputter coater, and observed with a JEOL JSM-6100 scanning electron microscope.

Transmission electron microscopy

Conventional chemical fixation and cryofixation were performed basically as described by Holstein et al. [61]. C*hemical fixation*: Hydra polyps were allowed to attach on a dialysis membrane, relaxed in 2 % urethane for 3 min and immediately fixed with a combined 2.5 % glutaraldehyde and 1 % osmium tetroxide fixative, dehydrated in a graded acetone series and embedded in Polybed 812 resin.

High pressure freezing (HPF) and freeze substitution

Basal discs were dissected and frozen with a HPM-010 (HPF apparatus from BAL-TEC, Baltzers, Liechtenstein), freeze substituted with acetone containing osmium tetroxide and uranyl acetate, and embedded into PolyBed 812 as previously described [61]. Thick sections (350 nm) and ultrathin sections (70 nm) were cut with a Leica ultramicrotome UCT (Leica, Austria), mounted on copper grids and stained with uranyl acetate and lead citrate and examined with a Zeiss Libra 120 energy filter transmission electron microscope using zero loss electrons. Images were taken with a TRS 2048 high speed camera (Tröndle, Germany) and visualized through Olympus SiS iTEM 5.0 software.

Cytochemical detection of PAS-positive 1–2 vicinal diols was carried out according to Thiery [63]. Sections from cryofixed samples were mounted on gold grids, exposed to periodic acid, thiocarbohydrazide, and silver proteinate. Negative control included omission of periodic acid treatment.

Peroxidase activity was detected in *Hydra* polyps fixed with 4 % PFA in 0.1 M PBS. They were stained with diamino benzidine (DAB + CHROMOGEN, Dako), and post fixation with 2.5 % glutaraldehyde/1 % osmium tetroxide, dehydration and embedding into Polybed 812. Images were taken without any further section post-staining. Controls included the inhibition of peroxidase activity by incubating samples in 3 % hydrogen peroxide for 20 min.

Electron energy loss spectroscopy (EELS) and electron spectroscopic imaging (ESI) were performed on ultrathin sections in order to detect element distribution in structures rich in nitrogen (N) and phosphorus (P) within the basal disc cells. The EELS charts and ESI images were collected using the software iTEM 5.0©. Distribution of N and P was measured according to a three-window power law difference ESI model with an energy slit width of 15 eV. Here, two background images and one image at the ionization edge of the appropriate element, K edge 397 eV for N and $L_{2,3}$ edge at 129 eV for P were taken. Maximum element distribution was finally mix mapped with an inverted high contrast image taken at 250 eV.

The window-one was placed at 382 eV, the window-two at 350 eV, and window-three at 410 eV. The difference of the three windows coincide with the onset of the N –K ionization edge at 397 eV. The background image was set with the subtraction model obtained from the EELS analyses default, which ensures that only the energy loss from the ion under examination is mapped. Likewise, for constructing the distribution map of P, the window-one was placed at 121 eV, window-two at 110, and window-three at 153 eV. The energy-loss contribution of three windows coincide with the onset of P $-L_{2,3}$ ionization edge of 129 eV.

Atomic force microscopy

Footprints from *Hydra* were collected on glass slides. The samples were let dry at room temperature and analyzed with Atomic Force Microscopy (AFM- Peak Force Tapping™, PFT). Data collection was achieved by applying controlled, low forces on the tip of the cantilever during imaging, which allows a direct comparison between the morphology and the adhesive properties at the nanometer (nm) scale. With the PFT method, an adhesion profile can be obtained by evaluating one force-distance curve for each pixel of the obtained image. Thereof, the adhesion force is defined as the maximum force needed to pull off the cantilever tip. The probe (silicon tip on silicon nitride cantilever—SNL, Bruker, Santa Barbara, CA, USA, k¼0.12 N/m) was calibrated on a stiff surface prior to the experiment for the measurements of the mechanical properties, in order to quantify the tip sample force.

Additional files

Additional file 1: *Hydra magnipapillata* dettaching from a glass slide in real time. (MP4 3304 kb)

Additional file 2: Phalloidin staining of actin filaments visualized with confocal microscopy. a overview of basal disc myoneme organization. The square indicates the area magnified in figure b. b detail of actin filaments in the basal disc. c lateral view of basal disc showing actin filaments which branched perpendicularly towards the apical side. Arrowheads point at actin filaments from basal disc cells, and arrows indicate the ones from endodermal cells. *Scale bars* 50 μm (a), 15 μm (b, c). *Abbreviation*: ap, aboral pore; m, mesoglea; bdc, ectodermal basal disc cells. (TIF 18280 kb)

Additional file 3: Transmission electron microscopy images of chemically fixed basal discs from *Hydra magnipapillata*. a 350 nm sections from longitudinal section of apical side of basal disc cell. Note that given the thickness of sections, overlapping secretory granules can be seen. b 350 nm sections from longitudinal section of basal side of basal disc cell. Myoneme branching towards the apical side are seen. c 70 nm section longitudinal section of basal disc showing possible HSGII developing stages. *Scale bars* 2 μm (a), 1 μm (b, c). *Abbreviations*: I, *Hydra* secretory granule I; II, *Hydra* secretory granule II; I/II, possible developing transition between HSGI and HSGII; III, *Hydra* secretory granule III; IV, *Hydra* secretory granule IV; ex, exterior of the cell; m, mesoglea; my, myoneme; er, endoplasmic reticulum; arrows, indicate cytoplasmic extensions; asterisks, indicate vacuoles of water; arrowheads, indicate myoneme branching towards apical side of basal disc cell. (TIF 9364 kb)

Additional file 4: Cytochemistry of *Hydra* basal disc. a longitudinal section of a basal disc stained with alcian blue. Basal disc cells did not react for acidic mucopolysaccarides. b Longitudinal section through a *Hydra* tentacle. Nematocytes were alcian blue positive (arrows) corroborating the method used was correct. *Scale bars* 100 μm (a), 50 μm (b). *Abbreviations*: bd, basal disc; m, mesoglea; en, endoderm (TIF 3667 kb)

Additional file 5: Lipidaceous granules distribution within *Hydra* basal disc. Whole mounts were stained with Nile Red. a-a''' *Hydra* polyps contain few scattered lipid droplets within basal disc cells. Unlike basal disc cells, the endoderm is rich in lipids. b-b''' negative control was established after a series of ETOH washes. *Scale bars* 30 μm. *Abbreviations*: bd, basal disc; m, mesoglea; en, endoderm (TIF 6150 kb)

Additional file 6: Electron spectral imaging (ESI), and electron energy loss spectroscopy (EELS) performed in sections of cryo-fixed basal disc. a Merged ESI micrographs revealing the nitrogen atoms profile –green dots. Nitrogen atoms are densely distributed in *Hydra* secretory granule II, covering its full surface. b Merged ESI micrographs depicting P atoms distribution –green dots. Note P atoms are found in the same secretory granules as N but in much lower density. *Scale bars* 1 μm. *Abbreviations*: ex, exterior of the cell. (TIF 2992 kb)

Abbreviations

AB, alcian blue; EELS, electron energy loss spectroscopy; EM, electron microscopy; ER, endoplasmic reticulum; ESI, electron spectroscopic imaging; HPF, high pressure freezing; HSG I-IV, Hydra secretory granule one to four; PAS, periodic acid Schiff

Acknowledgements

The authors are most grateful to Karin Gutleben and Thi Chinh Ngo for excellent assistance for high pressure freezing/freeze substitution, and atomic force microscopy, respectively. We are indebted to Marina P. Samoylovich, Yoshitaka Kobayakawa, and Alexander V. Klimovich for kindly providing the antibodies used in this study. We also thank Martin Offterdinger for support during SP8 experiments.

Funding

MR was supported by Marie-Curie FP7-PEOPLE-2013-IEF 626525 fellowship, and COST Action TD0906. The project was also supported by Austrian Science Fund (FWF) grant 25404-B25.

Availability of data and material

The datasets supporting the conclusions of this article are included within the article and its additional files.

Authors' contributions

MR and PLa conceived the study, performed experiments and wrote the paper. PLe performed and supervised AFM experiments. PF contributed to electron microscopy. MWH contributed to cryo-based electron microscopy and (immune) cytochemistry. WS performed histological and ultrastructural experiments. BH contributed on light microscopy, and cell macerations and Hydra biology. All authors have read and approved the manuscript.

Competing interests

The authors declare that they have no competing interests.

Consent for publication

Not applicable.

Ethics approval and consent to participate

Not applicable.

Author details

[1]Institute of Zoology and Center for Molecular Biosciences Innsbruck, University of Innsbruck, Innsbruck, Austria. [2]Laboratory for Chemistry of Novel Materials, Research Institute for Material Sciences and Engineering, Center of Innovation and Research in Materials and Polymers, University of Mons, Mons, Belgium. [3]Biology of Marine Organisms and Biomimetics, Research Institute for Biosciences, University of Mons, Mons, Belgium. [4]Division of Histology and Embryology, Innsbruck Medical University, Innsbruck, Austria.

Received: 12 October 2015 Accepted: 26 July 2016
Published online: 23 August 2016

References

1. Waite JH, Andersen NH, Jewhurst S, Sun C. Mussel adhesion: finding the tricks worth mimicking. J Adhes. 2005;81:297–317.
2. Jonker J-L, von Byern J, Flammang P, Waltraud K, Power AM. Unusual adhesive production system in the barnacle *Lepas anatifera*: an Ultrastructural and histochemical investigation. J Morphol. 2012;273:1377–91.
3. Zheden V, Klepal W, von Byern J, Bogner FR, Thiel K, Kowalik T, Grunwald I. Biochemical analyses of the cement float of the goose barnacle *Dosima fascicularis* – a preliminary study. Biofouling. 2014;30:949–63.
4. Hennebert E, Wattiez R, Demeuldre M, Ladurner P, Hwang DS, Waite JH, Flammang P. Sea star tenacity mediated by a protein that fragments, then aggregates. Proc Natl Acad Sci U S A. 2014;111:6317–22.
5. Lengerer B, Pjeta R, Wunderer J, Rodrigues M, Arbore R, Schärer L, Berezikov E, Hess MW, Pfaller K, Egger B, Obwegeser S, Salvenmoser W, Ladurner P. Biological adhesion of the flatworm *Macrostomum lignano* relies on a duo-gland system and is mediated by a cell type-specific intermediate filament protein. Front Zool. 2014;11:12.
6. Wang CS, Stewart RJ. Localization of the bioadhesive precursors of the sandcastle worm, *Phragmatopoma californica* (Fewkes). J Exp Biol. 2012; 215(Pt 2):351–61.
7. Demeuldre M, Chinh Ngo T, Hennebert E, Wattiez R, Leclère P, Flammang P. Instantaneous adhesion of Cuvierian tubules in the sea cucumber *Holothuria forskali*. Biointerphases. 2014;9:029016.
8. Smith AM, Callow JA. Biological Adhesives. Berlin: Springer Berlin Heidelberg; 2006.
9. von Byern J, Grunwald I. Biological Adhesive Systems. Vienna: Springer Vienna; 2010.
10. Flammang P, Michel A, Cauwenberge A, Alexandre H, Jangoux M. A study of the temporary adhesion of the podia in the sea star *Asterias rubens* (Echinodermata, asteroidea) through their footprints. J Exp Biol. 1998;201(Pt 16):2383–95.
11. Walker G. The biochemical composition of the cement of two barnacle species, *balanus hameri* and *balanus crenatus*. J Mar Biol Assoc U K. 1972;52: 429–35.
12. Bandara N, Zeng H, Wu J. Marine mussel adhesion: biochemistry, mechanisms, and biomimetics. J Adhes Sci Technol. 2013;27:2139–62.
13. Lee H, Dellatore SM, Miller WM, Messersmith PB. Mussel-inspired surface chemistry for multifunctional coatings. Science. 2007;318:426–30.
14. Becker PT, Lambert A, Lejeune A, Lanterbecq D, Flammang P. Identification, characterization, and expression levels of putative adhesive proteins from the tube-dwelling polychaete *Sabellaria alveolata*. Biol Bull. 2012;223:217–25.
15. Sagert J, Sun C, Waite JH. Chemical Subtleties of Mussel and Polychaete Holdfasts. In: Smith DAM, Callow DJA, editors. Biological Adhesives. Berlin: Springer Berlin Heidelberg; 2006. p. 125–43.
16. Flammang P, Lambert A, Bailly P, Hennebert E. Polyphosphoprotein-containing marine adhesives. J Adhes. 2009;85:447–64.
17. Hennebert E, Wattiez R, Flammang P. Characterisation of the carbohydrate fraction of the temporary adhesive secreted by the tube feet of the sea star *Asterias rubens*. Mar Biotechnol N Y N. 2011;13:484–95.
18. Quinn B, Gagné F, Blaise C. *Hydra*, a model system for environmental studies. Int J Dev Biol. 2012;56:613–25.
19. Steele RE. Developmental signaling in *hydra*: what does It take to build a "simple" animal? Dev Biol. 2002;248:199–219.
20. Lentz T. The Cell Biology of Hydra. Amsterdam: North-Holland publishing company; 1966.
21. Dübel S, Hoffmeister SA, Schaller HC. Differentiation pathways of ectodermal epithelial cells in *Hydra*. Differ Res Biol Divers. 1987;35:181–9.
22. Hobmayer B, Jenewein M, Eder D, Eder M-K, Glasauer S, Gufler S, Hartl M, Salvenmoser W. Stemness in *Hydra* - a current perspective. Int J Dev Biol. 2012;56:509–17.
23. Bode HR. Axial patterning in *hydra*. Cold Spring Harb Perspect Biol. 2009;1: a000463.
24. Holstein TW, Hobmayer E, Technau U. Cnidarians: an evolutionarily conserved model system for regeneration? Dev Dyn. 2003;226:257–67.
25. Bosch TCG. *Hydra* and the evolution of stem cells. BioEssays. 2009;31:478–86.
26. Bosch TCG. Why polyps regenerate and we don't: towards a cellular and molecular framework for *hydra* regeneration. Dev Biol. 2007;303:421–33.
27. Chaet AB. Invertebrate adhering surfaces: secretions of the starfish, *Asterias forbesi*, and the coelenterate, *Hydra pirardi*. Ann N Y Acad Sci. 1965;118:921–9.
28. Philpott DE, Chaet AB, Burnett AL. A study of the secretory granules of the basal disk of *Hydra*. J Ultrastruct Res. 1966;14:74–84.
29. Davis LE. Histological and ultrastructural studies of the basal disk of *Hydra*. Z Für Zellforsch Mikrosk Anat. 1973;139:1–27.

30. Hoffmeister-Ullerich SAH, Herrmann D, Kielholz J, Schweizer M, Schaller HC. Isolation of a putative peroxidase, a target for factors controlling foot-formation in the coelenterate *Hydra*. Eur J Biochem. 2002;269:4597–606.
31. Pan HC, Yang HQ, Zhao FX, Qian XC. Molecular cloning, sequence analysis, prokaryotic expression, and function prediction of foot-specific peroxidase in *Hydra magnipapillata* Chinese strain. Genet Mol Res. 2014;13:6610–22.
32. Rodrigues M, Lengerer B, Ostermann T, Ladurner P. Molecular biology approaches in bioadhesion research. Beilstein J Nanotechnol. 2014;5:983–93.
33. Alibardi L, Edward D, Patil L, Bouhenni R, Dhinojwala A, Niewiarowski P. Histochemical and ultrastructural analyses of adhesive setae of lizards indicate that they contain lipids in addition to keratins. J Morphol. 2011;272:758–68.
34. Gohad NV, Aldred N, Hartshorn CM, Jong Lee Y, Cicerone MT, Orihuela B, Clare AS, Rittschof D, Mount AS. Synergistic roles for lipids and proteins in the permanent adhesive of barnacle larvae. Nat Commun. 2014;5:4414.
35. Amano H, Koizumi O, Kobayakawa Y. Morphogenesis of the atrichous isorhiza, a type of nematocyst, in *Hydra* observed with a monoclonal antibody. Dev Genes Evol. 1997;207:413–6.
36. Kobayakawa Y, Kodama R. Foot formation in *Hydra*: commitment of the basal disk cells in the lower peduncle. Dev Growth Differ. 2002;44:517–26.
37. Shirokova VN, Begas OS, Knyazev NA, Samoilovich MP. Antigenic marker of differentiated cells of a *Hydra* basal disc. Cell Tissue Biol. 2009;3:84–92.
38. Whittington ID, Armstrong WD, Cribb BW. Mechanism of adhesion and detachment at the anterior end of *Neoheterocotyle rhinobatidis* and *Troglocephalus rhinobatidis* (Monogenea: Monopisthocotylea: Monocotylidae). Parasitol Res. 2004;94:91–5.
39. Hennebert E, Viville P, Lazzaroni R, Flammang P. Micro- and nanostructure of the adhesive material secreted by the tube feet of the sea star *Asterias rubens*. J Struct Biol. 2008;164:108–18.
40. Xia L, Lenaghan SC, Zhang M, Wu Y, Zhao X, Burris Jr JN, Stewart Jr CN. Characterization of English ivy (*Hedera helix*) adhesion force and imaging using atomic force microscopy. J Nanoparticle Res. 2010;13:1029–37.
41. von Byern J, Klepal W. Adhesive mechanisms in cephalopods: a review. Biofouling. 2006;22:329–38.
42. Flammang P. Adhesive Secretions in Echinoderms: An Overview. In: Smith DAM, Callow DJA, editors. Biological Adhesives. Berlin: Springer Berlin Heidelberg; 2006. p. 183–206.
43. Smith AM. Gastropod Secretory Glands and Adhesive Gels. In: von Byern DD-BJ, Grunwald DD-BI, editors. Biological Adhesive Systems. Vienna: Springer; 2010. p. 41–51.
44. Silverman HG, Roberto FF. Understanding marine mussel adhesion. Mar Biotechnol N Y N. 2007;9:661–81.
45. Stewart RJ, Ransom TC, Hlady V. Natural underwater adhesives. J Polym Sci Part B Polym Phys. 2011;49:757–71.
46. Stewart RJ, Wang CS. Adaptation of caddisfly larval silks to aquatic habitats by phosphorylation of H-fibroin serines. Biomacromolecules. 2010;11:969–74.
47. Waite JH, Qin X. Polyphosphoprotein from the adhesive pads of *Mytilus edulis*†. Biochemistry (Mosc). 2001;40:2887–93.
48. Zhao H, Sun C, Stewart RJ, Waite JH. Cement proteins of the tube-building polychaete *phragmatopoma californica*. J Biol Chem. 2005;280:42938–44.
49. Petrone L, Easingwood R, Barker MF, McQuillan AJ. In situ ATR-IR spectroscopic and electron microscopic analyses of settlement secretions of *Undaria pinnatifida* kelp spores. J R Soc Interface. 2011;8:410–22.
50. Engholm-Keller K, Larsen MR. Technologies and challenges in large-scale phosphoproteomics. Proteomics. 2013;13:910–31.
51. Jensen ON. Interpreting the protein language using proteomics. Nat Rev Mol Cell Biol. 2006;7:391–403.
52. Hand AR. Ultrastructural localization of catalase and L-alpha-hydroxy acid oxidase in microperoxisomes of *Hydra*. J Histochem Cytochem. 1976;24:915–25.
53. Hoffmeister S, Schaller HC. A new biochemical marker for foot-specific cell differentiation in *Hydra*. Wilhelm Rouxs Arch Dev Biol. 1985;194:453–61.
54. Chapman JA, Kirkness EF, Simakov O, Hampson SE, Mitros T, Weinmaier T, Rattei T, Balasubramanian PG, Borman J, Busam D, Disbennett K, Pfannkoch C, Sumin N, Sutton GG, Viswanathan LD, Walenz B, Goodstein DM, Hellsten U, Kawashima T, Prochnik SE, Putnam NH, Shu S, Blumberg B, Dana CE, Gee L, Kibler DF, Law L, Lindgens D, Martinez DE, Peng J, et al. The dynamic genome of *Hydra*. Nature. 2010;464:592–6.
55. Böttger A, Doxey AC, Hess MW, Pfaller K, Salvenmoser W, Deutzmann R, Geissner A, Pauly B, Altstätter J, Münder S, Heim A, Gabius H-J, McConkey BJ, David CN. Horizontal gene transfer contributed to the evolution of extracellular surface structures: the freshwater polyp *hydra* is covered by a complex fibrous cuticle containing glycosaminoglycans and proteins of the PPOD and SWT (sweet tooth) families. PLoS ONE. 2012;7.
56. Technau U, Miller MA, Bridge D, Steele RE. Arrested apoptosis of nurse cells during *Hydra* oogenesis and embryogenesis. Dev Biol. 2003;260:191–206.
57. Wang C-S, Ashton NN, Weiss RB, Stewart RJ. Peroxinectin catalyzed dityrosine crosslinking in the adhesive underwater silk of a casemaker caddisfly larvae, *Hysperophylax occidentalis*. Insect Biochem Mol Biol. 2014;54:69–79.
58. Weis VM, Small AL, McFall-Ngai MJ. A peroxidase related to the mammalian antimicrobial protein myeloperoxidase in the Euprymna–Vibrio mutualism. Proc Natl Acad Sci. 1996;93:13683–8.
59. Hobmayer B, Holstein TW, David CN. Stimulation of tentacle and bud formation by the neuropeptide head activator in *Hydra magnipapillata*. Dev Biol. 1997;183:1–8.
60. Richardson KC, Jarett L, Finke EH. Embedding in epoxy resins for ultrathin sectioning in electron microscopy. Biotech Histochem. 1960;35:313–23.
61. Holstein TW, Hess MW, Salvenmoser W. Preparation techniques for transmission electron microscopy of *Hydra*. Methods Cell Biol. 2010;96:285–306.
62. Tokuyasu KT. A technique for ultracryotomy of cell suspensions and tissues. J Cell Biol. 1973;57:551–65.
63. Thiéry J. Mise en évidence des polysaccharides sur coupes fines en microscopie électronique. J Microsc. 1967;6:987–1018.